

Received June 17, 2020, accepted July 15, 2020, date of publication August 5, 2020, date of current version September 24, 2020.

Digital Object Identifier 10.1109/ACCESS.2020.3014407

Continuous Multi-Scroll Chaotic PWM and Its Chaotic Signal Selection Method for EMI Suppression of Power Converters

ZHICHANG YANG¹, (Graduate Student Member, IEEE), HONG LI¹, (Senior Member, IEEE), YUHANG DING¹, AND JIAXIN WANG¹

School of Electrical Engineering, Beijing Jiaotong University, Beijing 100044, China

Corresponding author: Hong Li (hli@bjtu.edu.cn)

This work was supported in part by the Excellent Youth Scholars of National Natural Science Foundation of China under Grant 51822701, and in part by the Key Project of National Natural Science Foundation of China under Grant U1866211.

ABSTRACT Chaotic pulse width modulation (PWM) technique has been applied to suppress electromagnetic interference (EMI) in power converters. However, traditional discrete chaotic PWM has the shortcoming that the spreading spectrum distribution is triangular in shape and the practical spreading frequency bandwidth is much larger than the designed, which will further result in the limited EMI suppression. In this paper, a continuous chaotic PWM method based on the continuous multi-scroll chaotic attractors is put forward to suppress EMI more effectively, getting better spread spectrum distribution at switching frequency and its multiples for power converters. Moreover, to guide the selection of chaotic signals in real applications, the influence mechanism of multi-scroll chaotic signals on EMI spectrum distribution is firstly analyzed in this paper so as to provide a practical chaotic signal selection method. Finally, the experiments are presented followed by the simulations on a boost converter to verify the effectiveness of the proposed continuous multi-scroll chaotic PWM method and the correctness of the given chaotic signal selection method. This paper provides design guidance for the chaotic PWM in engineering applications.

INDEX TERMS Electromagnetic interference, power converters, chaotic pulse width modulation, multi-scroll chaotic attractors, spectral characteristics.

I. INTRODUCTION

With the more and more strict requirements on high power density and high reliability, electromagnetic interference (EMI) suppression is becoming a key issue in power converters, especially with the extensive use of wide bandgap semiconductor devices [1]–[4]. Chaotic pulse width modulation (PWM) provides an effective solution for EMI suppression in power converters relying on changing the switching frequency with chaotic behaviours, which will shape the spectrum distribution of EMI sources and reduce the peaks of EMI spectrum distributed at the switching frequency and its multiples [5]–[7].

Chaotic PWM is to suppress EMI based on modulation technology of power converters, which has the advantages of no increase of external hardware and no increase of the volume, weight, and cost of power converters [8]–[11]. Thus,

The associate editor coordinating the review of this manuscript and approving it for publication was Mohamed Kheir¹.

chaotic PWM has been studied extensively and lots of valuable achievements have been obtained [12]–[19]. Different chaotic PWMs have been applied to various types of power converters to suppress conducted EMI, such as DC-DC converters, AC-DC converters, motor drive systems, etc., which not only can effectively reduce the peaks of EMI, but also largely reduce the volume and cost of the EMI filters in power converters [12]–[15]. The chaotic spectrum calculation method with chaotic PWM of power converters have been presented in the literature [16], [17]. In [18], [19], the output voltage ripple, power losses, and other performances of power converters under chaotic PWM have further been analyzed in detail, there is a tradeoff between EMI reduction and output ripple, but the power losses will be influenced lightly. The current research results have entirely shown the effectiveness and practicability of chaotic PWM in real engineering.

The remaining problem is how to select a right and better chaotic signal for chaotic PWM in real applications since different chaotic signals will result in different spread spectrum

distribution and different effects of EMI suppression. Traditionally, the discrete chaotic mappings are usually used in chaotic PWM as frequency modulated signals, but the chaotic signals generated by the discrete chaotic mappings have a strong jump characteristic, which limits the EMI suppression effect of chaotic PWM for power converters [20]. Moreover, the practical spreading frequency bandwidth is much larger than the designed frequency band under traditional chaotic PWM (TC-PWM) with discrete chaotic mappings, and it could lead to unwanted sideband noise [21].

In recent decades, the theory of continuous chaotic system has been developing quickly. The representatives of continuous chaotic systems are Lorenz family [22], Chua system [23], Chen system [24], Lü system [25], Ruchlidge system [26] and so on. These chaotic systems can also be classified into the multi-scroll system, multi-loop system, multi-wing system based on the topological structure of the phase diagram [27]. For example, Chua's circuit is a double scroll system, and the multi-scroll system with multi-direction can be obtained based on the framework of Chua's circuit though replacing the original piecewise linear function with different nonlinear functions [28]. From the variety of phase diagrams, the multi-scroll systems have more richly chaotic dynamic behaviors compared with discrete chaotic mappings. Thus, the proposed multi-scroll systems provide the possibility to realize a better EMI suppression than that under the existing TC-PWM. Chua's circuit with analog implementation was firstly applied to generate a chaotic carrier for the EMI suppression in DC-DC converters in [29]. In the literature, there is lack of a method or index for systematically evaluating the impact of the multi-scroll chaotic PWM (MC-PWM) with different chaotic signals on EMI spectrum distribution, i.e., there is no chaotic signal selection method for MC-PWM. However, it is very important to find the optimal MC-PWM for the real engineering applications, since it directly influences if the converter can pass EMC standard.

To solve the above problems, the MC-PWM with the continuous multi-scroll chaotic system is proposed for EMI suppression of power converters in Section II. Following, the influence mechanism of MC-PWM signals on spectrum distribution of EMI is documented, and a concept of average relative variation (ARV) of the chaotic signals is defined. Based on ARV, the method of selecting chaotic signals for MC-PWM is given in Section III. The simulation comparison of EMI suppression effect on a boost converter under MC-PWM with different ARV is provided in Section IV. In Section V, experimental results are presented to verify the effectiveness of EMI suppression under MC-PWM and the correctness of the given chaotic signal selection method. Finally, the conclusions are drawn in Section VI.

II. REALIZATION OF MC-PWM IN POWER CONVERTERS

A. REALIZATION OF MC-PWM IN POWER CONVERTERS

It is well known that the trains of switched pulses are commonly generated by comparing a reference waveform with a

higher frequency carrier in PWM control for power converters. The switching frequency is a fixed value for traditional PWM (T-PWM). For chaotic PWM, the switching frequency is changing with chaotic behaviours within a certain range according to a kind of discrete chaotic mappings or continuous chaotic systems. Because the switching frequency is the reciprocal of carrier period, the carrier period T_k of chaotic PWM can be expressed by (1), where T_r is the reference switching period, ΔT is the maximum period offset, and ε_k is the modulation signal, and it is generated by chaotic mappings or chaotic systems.

$$T_k = T_r + \Delta T \cdot \varepsilon_k, \varepsilon_k \in (-1, 1), \quad k = 1, 2, \dots \quad (1)$$

From (1), it can be obtained that ε_k determines the changing regularity of switching period, which can further shape the spectral distribution of EMI sources, so the key of chaotic PWM to suppress EMI is to select an appropriate modulation signal ε_k . Usually, discrete chaotic mappings, such as Logistic mapping, Tent mapping, Chebyshev mapping, are applied into chaotic PWM as the modulation signals to realize TC-PWM in power converters [30].

The EMI peaks could be reduced using TC-PWM with discrete chaotic mappings. However, chaotic dynamical behaviours of the discrete chaotic mappings are relatively simple and the chaotic signals generated by the discrete chaotic mappings have a strong jump characteristic, which results in a limited effect on EMI suppression and the unwanted spreading frequency bandwidth for power converters. Therefore, the TC-PWM should be optimized to overcome the increasingly severe EMI problem of power converters.

The proposed MC-PWM is realized by introducing the multi-scroll chaotic attractors into chaotic PWM based on the theory of continuous chaotic systems. The ε_k in (1) is generated by sampling the state variable of $n \times m$ -scroll attractors of chaotic systems, and then the range of signal values is bounded from -1 to 1 by uniform scaling. The realization process of MC-PWM is shown in Fig. 1. Firstly, the ε_k should be generated by sampling one of the state variables of $n \times m$ -scroll attractors with sampling period T_{samp} . Then the ε_k will be used to generate carrier period base on (1), correspondingly, the carrier period will follow the changing regularity of ε_k . Finally, the trains of switched pulses of power

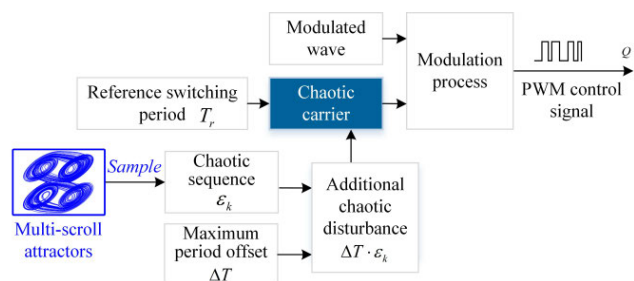


FIGURE 1. Block diagram of the MC-PWM realization.

switches will be formed by comparing modulated wave and chaotic carrier, which means power converters are working under MC-PWM.

B. GENERATION OF MULTI-SCROLL CHAOTIC ATTRACTORS

The key issue of MC-PWM is to generate multi-scroll chaotic attractors as chaotic modulation signals. So, the realization and characteristics of multi-scroll chaotic attractors will be presented. Multi-scroll chaotic attractors can be generated by modified Chua’s circuits, modified Jerk circuit and other chaotic systems by replacing the original piecewise linear function with different nonlinear functions [27]. The modified Chua’s circuit is applied to MC-PWM to generate multi-scroll chaotic attractors in this paper.

The dimensionless state equation of the modified Chua’s circuit is presented as (2) [28]:

$$\begin{cases} \dot{x} = \alpha [y - f_2(y) - f_1(x, \xi)] \\ \dot{y} = x - y + z \\ \dot{z} = -\beta [y - f_2(y)] \end{cases} \quad (2)$$

where α , β , and ξ are the control parameters of the modified Chua’s circuit. The $f_1(x, \xi)$ and $f_2(y)$ are two nonlinear piecewise functions. To generate even attractors in the horizontal coordinates, $f_1(x, \xi)$ in (2) can be defined as (3), where the number of attractors $n = 2N$. Moreover, to generate odd attractors in the horizontal coordinates, $f_1(x, \xi)$ can be defined as (5), where the number of attractors $n = (2N + 1)$.

$$f_1(x, \xi) = \xi \left\{ x - A_1 \begin{bmatrix} -\operatorname{sgn}(x) + \sum_{i=0}^{N-1} \operatorname{sgn}(x + 2iA_1) \\ + \sum_{i=0}^{N-1} \operatorname{sgn}(x - 2iA_1) \end{bmatrix} \right\}, \quad A_1 > 0, \quad N \geq 1. \quad (3)$$

where

$$\operatorname{sgn}(x) = \begin{cases} 1 & \text{if } x > 0 \\ 0 & \text{if } x = 0 \\ -1 & \text{if } x < 0 \end{cases} \quad (4)$$

$$f_1(x, \xi) = \xi \left\{ x - A_1 \begin{bmatrix} \sum_{i=0}^{N-1} \operatorname{sgn}(x + (2i + 1)A_1) \\ + \sum_{i=0}^{N-1} \operatorname{sgn}(x - (2i + 1)A_1) \end{bmatrix} \right\}, \quad A_1 > 0, \quad N \geq 1. \quad (5)$$

To generate even attractors in the vertical coordinates, $f_2(y)$ in (2) is defined as (6), where the number of attractors $m = 2M$. Moreover, to generate odd attractors in the vertical coordinates, $f_2(y)$ is defined as (7), where the number of

attractors $m = (2M + 1)$.

$$f_2(y) = A_2 \left[\begin{aligned} & -\operatorname{sgn}(y) + \sum_{j=0}^{M-1} \operatorname{sgn}(y + 2jA_2) \\ & + \sum_{j=0}^{M-1} \operatorname{sgn}(y - 2jA_2) \end{aligned} \right], \quad A_2 > 0, \quad M \geq 1. \quad (6)$$

Or

$$f_2(y) = A_2 \left[\begin{aligned} & \sum_{j=0}^{M-1} \operatorname{sgn}(y + (2j + 1)A_2) \\ & + \sum_{j=0}^{M-1} \operatorname{sgn}(y - (2j + 1)A_2) \end{aligned} \right], \quad A_2 > 0, \quad M \geq 1. \quad (7)$$

In (2), α , β and ξ are the control parameters of the modified Chua’s circuit system, by adjusting these parameters, the modified Chua’s circuit system can operate in chaotic mode. For example, the bifurcation diagram of x versus ξ is shown in Fig. 2. The state of the modified Chua’s circuit system can be determined based on the bifurcation diagram. Therefore, the selected α , β and ξ need to ensure that the system is operating in chaos. A_1 and A_2 are used to control the position and size of the scroll of the modified Chua’s circuit system. So the determination of A_1 and A_2 is based on the distribution range of the required state variable. In this paper, the 2×2 -scroll attractor is generated to use in MC-PWM. The control parameters are set as $\alpha = 10$, $\beta = 16$, $\xi = 0.25$ to ensure that the system is in a chaotic state. Moreover, the A_1 and A_2 are set as $A_1 = 0.5$, $A_2 = 0.25$, the generated state variable x in (2) is distributed on the required range $(-1, 1)$. Finally, The generated 2×2 -scroll attractor is shown in Fig. 3.

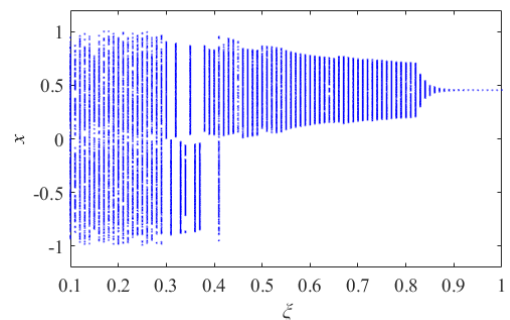


FIGURE 2. Bifurcation diagram of x with ξ .

III. INFLUENCE MECHANISM OF MC-PWM ON SPECTRUM DISTRIBUTION OF EMI

A. EMI ANALYSIS FOR POWER CONVERTERS

For power converters, PWM waveforms generated by high frequency switching processes are important sources of EMI. Especially with the applications of wide bandgap semiconductor devices with high frequencies and high power, the EMI

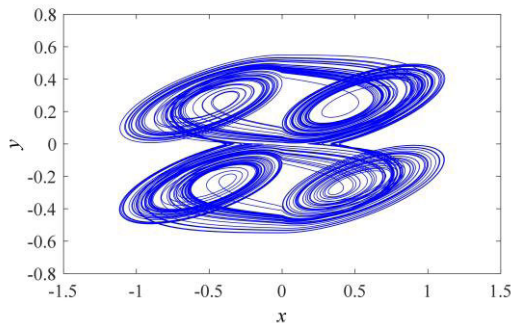


FIGURE 3. 2×2 -scroll ($N = 1, M = 1$) generated from (2) with f_1 and f_2 defined as (3) and (6).

problems will be more serious in power converters. The EMI of power converters can be divided into common-mode (CM) EMI and differential-mode (DM) EMI according to the EMI current flow paths [31].

In this paper, the boost converter, one of the most common DC-DC converters, is taken as an example to analyze the EMI problem of power converters. The topology of the boost converter and its CM EMI current and DM EMI current paths are shown in Fig. 4, where C_p represents the parasitic capacitor between the MOSFET Q and the heat sink. While L_{LN} , C_{LN} , and R_{LN} form the line impedance stabilization network (LISN). When the boost converter is running, there is DM current with high frequency flows through the MOSFET Q , and the LISN, which will result in DM EMI in the boost converter. At the same time, there is a high frequency CM current flows through parasitic capacitance to the earth and returns via LISN, which will lead to the CM EMI in the boost converter. Both DM EMI and CM EMI make the boost converter face serious EMI problems.

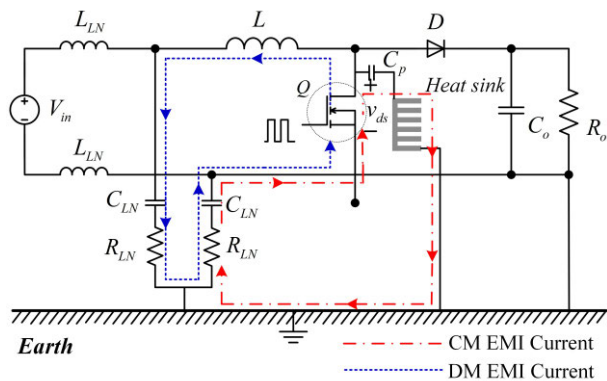


FIGURE 4. The boost converter topology and its EMI current paths.

According to EMI current paths shown in Fig. 4, the equivalent circuit of CM EMI and DM EMI can be obtained as shown in Fig. 5. It should be noted that the capacitor C_{LN} is not included in the equivalent circuit of CM EMI and DM EMI, because the C_{LN} can be regarded as

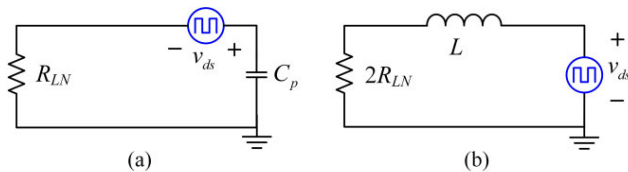


FIGURE 5. Equivalent circuit of conducted EMI. (a) Equivalent circuit of CM EMI. (b) Equivalent circuit of DM EMI.

a short circuit in the frequency band 150kHz~30MHz of conducted EMI test. Based on Fig. 5, it is obvious that the drain-source voltage v_{ds} of the switch Q is the EMI source. Based on the realization process of the proposed MC-PWM in Section II-A, the switching frequency of the boost converter under MC-PWM is changing with chaotic behaviours within a certain range according to the chaotic attractors. Thus, the spectrum of v_{ds} will spread over a wider frequency range around the switching frequency and its multiples, and the peaks of v_{ds} spectrum will be decreased accordingly. Further, the peaks of conducted EMI can be reduced according to Fig. 5. Since the innovation of this paper lies in the influence analysis of MC-PWM on EMI of the power converters, the influence of the parasitic parameters caused by PCB layout and mechanical structure on the EMI equivalent circuit is not mentioned in this paper.

B. SPECTRUM QUANTIZATION OF EMI UNDER MC-PWM

To analyze the EMI suppression mechanism in power converters with MC-PWM, the quantization method of the EMI spectrum is proposed based on Fourier transform theory.

According to the realization of MC-PWM, as shown in Fig. 1, the drain-source voltage v_{ds} of the switch is determined by comparing the reference waveform v_m with the chaotic carrier v_c , which is shown in Fig. 6, where T_k is the period of the k^{th} switching cycle. τ_k is the begin time of the k^{th} switching cycle, and it can be expressed as (8). V_o is the output voltage of the boost converter. P is the number of switching cycles. D is the duty ratio of the drive signal of the

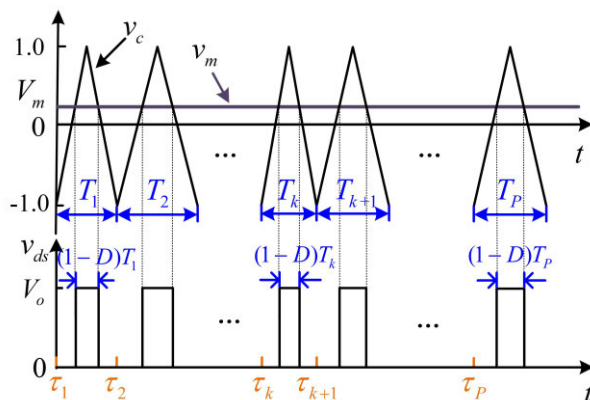


FIGURE 6. Generated principle of the v_{ds} under MC-PWM.

switch, then the duty ratio of v_{ds} can be expressed as $1-D$. The D is constant if the v_m is regarded as a constant value V_m in the boost converter.

$$\tau_k = \sum_{i=0}^{k-1} T_i, \quad k = 1, 2, 3, \dots, T_0 = 0. \quad (8)$$

Thus, the v_{ds} can be expressed as (9).

$$v_{ds}(t) = \lim_{P \rightarrow \infty} V_o \cdot \sum_{k=1}^P g_k(t - \tau_k) \quad (9)$$

where the $g_k(t)$ is defined as (10), and it denotes a pulse with different periods and the same duty ratio.

$$g_k(t) = \begin{cases} 1, & \text{for } \frac{D}{2}T_k \leq t < \left(1 - \frac{D}{2}\right)T_k. \\ 0, & \text{elsewhere.} \end{cases} \quad (10)$$

Because the $v_{ds}(t)$ is not a periodic signal, the Fourier transform theory is adopted to analyze frequency domain characteristics of $v_{ds}(t)$. According to the linearity property and the time-shifting property of the Fourier transform [32], the Fourier transform of $v_{ds}(t)$ is expressed as (11).

$$S_v(f) = \lim_{P \rightarrow \infty} V_o \cdot \sum_{k=1}^P G_k(f) e^{-2\pi f \tau_k} \quad (11)$$

where $G_k(f)$ denotes the Fourier transform of $g_k(t)$. The general expression of $G_k(f)$ is:

$$G_k(f) = (1 - D) T_k \cdot \text{sinc}[\pi f(1 - D)T_k] \cdot e^{-j\pi f T_k} \quad (12)$$

By substituting (1), (8), and (12) into (11), the Fourier transform of $v_{ds}(t)$ under MC-PWM is expressed as (13), where, ε_0 is defined as $\varepsilon_0 = 0$.

$$\begin{aligned} S_v(f) &= \lim_{P \rightarrow \infty} V_o \cdot \sum_{k=1}^P \\ &\times \left\{ (1-D)(T_r + \Delta T \varepsilon_k) \cdot \text{sinc}[\pi f(1 - D)(T_r + \Delta T \varepsilon_k)] \right. \\ &\left. \cdot e^{-j2\pi f \left[\left(k - \frac{1}{2}\right)T_r + \Delta T \left(\sum_{i=0}^{k-1} \varepsilon_i + \frac{\varepsilon_k}{2}\right) \right]} \right\} \quad (13) \end{aligned}$$

Because observation time is finite in the FFT analysis process, and the scanning time is also finite in the EMC test, the P is usually set to a finite value in practical applications. In such a case, the $v_{ds}(t)$ could be considered as a periodic signal with a period $T_c = \sum_{k=1}^P T_k$. When the P is large enough, it can reflect the characteristics of chaotic signals comprehensively. The minimum value of the P could be determined by the reference switching period T_r and the scanning time T_{scan} . The calculation formula is expressed in (14).

$$P = T_{scan} / T_r \quad (14)$$

Then, the Fourier transform of $v_{ds}(t)$ can be written as

$$\begin{aligned} S_v(f) &= F_c V_o \cdot \sum_{n=-\infty}^{\infty} \\ &\times \sum_{k=1}^P \left\{ \begin{aligned} &(1 - D)(T_r + \Delta T \varepsilon_k) \cdot \\ &\text{sinc}[\pi n F_c(1 - D)(T_r + \Delta T \varepsilon_k)] \\ &\cdot e^{-j2\pi n F_c \left[\left(k - \frac{1}{2}\right)T_r + \Delta T \left(\sum_{i=0}^{k-1} \varepsilon_i + \frac{\varepsilon_k}{2}\right) \right]} \end{aligned} \right\} \delta(f - n F_c) \quad (15) \end{aligned}$$

where $F_c = 1/T_c$. The spectra distribution of $v_{ds}(t)$ under MC-PWM can be obtained by (15).

To verify the correctness of (15), the calculated spectrum of $v_{ds}(t)$ using (15) will be compared with the simulated spectrum using the FFT analysis tool of MATLAB/Simulink. To clearly show each harmonic distribution, the P is set to a smaller value as $P = 100$. The other parameters are listed in TABLE 1. The comparison results are shown in Fig. 7, which indicates that the theoretical calculation and simulation results are consistent. That is, the proposed spectrum quantization method is correct.

TABLE 1. System parameters.

Parameter	Value
Input voltage	40 V
Rated power	300 W
Output voltage	100 V
Reference switching period T_r	1e-5 s
Maximum period offset ΔT	0.1T _r

C. INFLUENCE MECHANISM OF MC-PWM SIGNALS ON SPECTRUM DISTRIBUTION OF EMI

According to the Fourier transform of $v_{ds}(t)$ under MC-PWM, as expressed in (15), the main influencing factors of spectrum distribution of $v_{ds}(t)$ are the maximum period offset ΔT and modulation signal ε_k . Obviously, the spectrum peaks are lower when the ΔT is larger for the same ε_k . Thus, the influence of ε_k on spectrum distribution is analyzed below.

The probability density of ε_k is generally considered to be the main factor in determining the spectrum distribution [8]. However, even if the probability density is the same, the ε_k with different combinations and permutations will result in a very different spectrum distribution. For instance, three chaotic signals ε_k are obtained by sampling the 2×2 -scroll attractor as shown in Fig.3, the sampling period are *Case I*: $T_{samp} = 1.0s$, *Case II*: $T_{samp} = 0.2s$, and *Case III*: $T_{samp} = 0.02s$. Three ε_k have almost identical probability density as shown in Fig. 8. The spectra of $v_{ds}(t)$ around the switching frequency are shown in Fig. 9.

The magnitude and spreading bandwidth (SBW) of spectra around the switching frequency are marked in Fig. 9, which indicate that the magnitude and SBW are different with

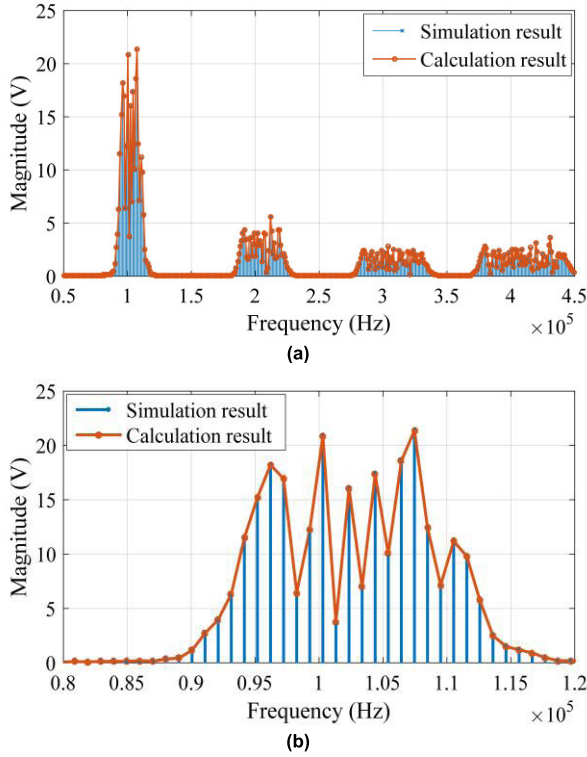


FIGURE 7. Comparison of calculation result and simulation of spectra of $v_{ds}(t)$ under chaotic PWM. (a) Frequency range 50kHz~450kHz. (b) Frequency range 80kHz~120kHz.

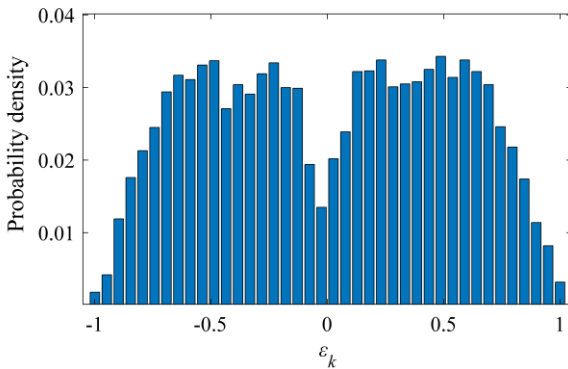


FIGURE 8. Probability density of ϵ_k .

different chaotic signals. The SBW in this paper means the spreading bandwidth of the spectrum around the switching frequency f_{sw} or its multiples under chaotic PWM. SBW_m is defined to distinguish the SBW at different frequencies $m \cdot f_{sw}$, where, m is the multiple of the switching frequency. The calculation of SBW_m is introduced as follows by using the spectra diagram of T-PWM and chaotic PWM as shown in Fig. 10, where h_{T_m} is the harmonic of the spectrum at the $m \cdot f_{sw}$ under T-PWM, $h_{c_m}(i)$ is the harmonic of the spectrum at each spreading frequency around the $m \cdot f_{sw}$ under chaotic PWM, $A_{c_m}(i)$ is the magnitude of $h_{c_m}(i)$, $f_{c_m}(i)$ is the frequency of $h_{c_m}(i)$, Based on Fig. 10, it can be known

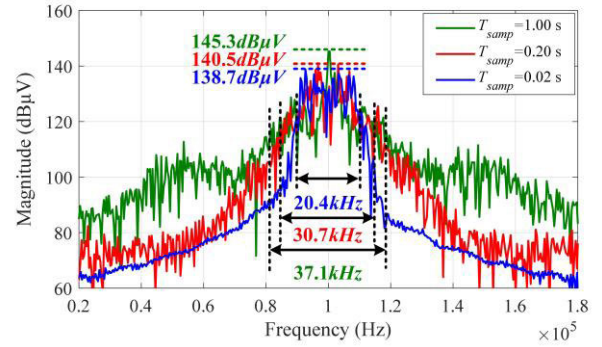


FIGURE 9. Spectra of $v_{ds}(t)$ around the switching frequency under MC-PWM.

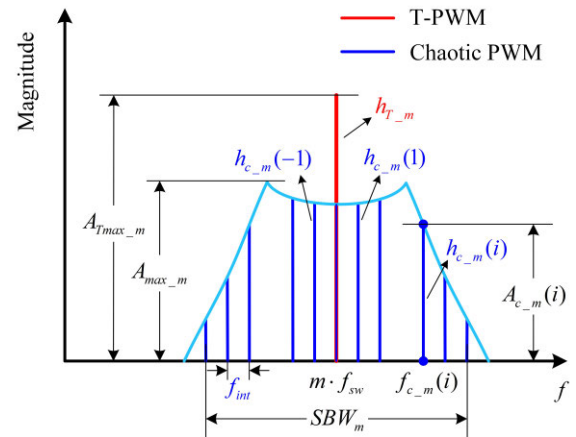


FIGURE 10. Spectra diagram of T-PWM and chaotic PWM.

that $f_{c_m}(i) = m \cdot f_{sw} + i \cdot f_{int}$, where f_{int} is the frequency interval of $h_{c_m}(i)$. According to the harmonics energy relationship between T-PWM and chaotic PWM around the $m \cdot f_{sw}$, when the (16) is satisfied, the frequency bandwidth $2N_{BW_m} \cdot f_{int}$ is determined as SBW_m , where N_{BW_m} means the harmonic number from $m \cdot f_{sw}$ to the frequency at which (16) will be satisfied, $E_{c_m}(i) = A_{c_m}^2(i)$ and $E_{T_m} = A_{T_{max_m}}^2$.

$$\sum_{i=-N_{BW_m}}^{N_{BW_m}} E_{c_m}(i) = 0.99 \cdot E_{T_m} \quad (16)$$

Fig. 9 indicates that the spectrum distribution cannot be analyzed accurately by the probability density of the ϵ_k . Therefore, the impact factor of EMI spectrum distribution should be found to reflect the distribution characteristics of the EMI spectrum and guide the selection of chaotic signals.

In this paper, the variation of adjacent signals δ_{ϵ_k} is firstly defined to denote the various level of ϵ_k . The expression of δ_{ϵ_k} is defined as (17).

$$\delta_{\epsilon_k} \triangleq \epsilon_{k+1} - \epsilon_k \quad (17)$$

According to (17), all ϵ_k can be represented by ϵ_1 and δ_{ϵ_k} as shown in (18). Hence, (15) can further be rewritten as (19),

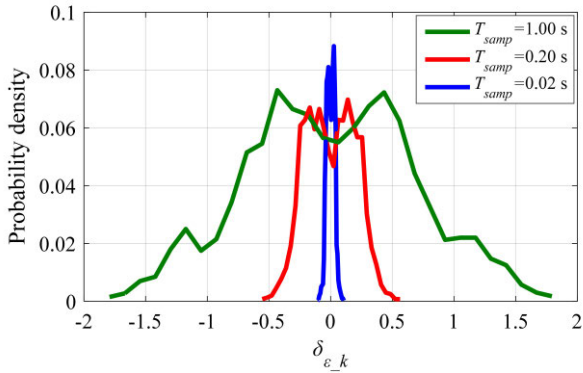


FIGURE 11. Probability density of δ_{ε_k} under different T_{samp} .

which means that the values of δ_{ε_k} determine spectral characteristics of $v_{ds}(t)$.

$$\varepsilon_k = \varepsilon_1 + \sum_{i=0}^{k-1} \delta_{\varepsilon_i}, \quad \delta_{\varepsilon_0} = 0. \quad (18)$$

$$S_v(f) = F_c V_o \cdot \sum_{n=-\infty}^{\infty} \sum_{k=1}^P \left\{ \begin{aligned} & (1-D)(T_r + \Delta T \varepsilon_k) \cdot \text{sinc}[\pi n F_c (1-D)(T_r + \Delta T \varepsilon_k)] \\ & \times e^{-j2\pi n F_c \left[\left(k - \frac{1}{2}\right) \cdot (T_r + \Delta T \varepsilon_1) + \Delta T \cdot \sum_{i=0}^{k-1} \left(k - i - \frac{1}{2}\right) \delta_{\varepsilon_i} \right]} \end{aligned} \right\} \delta(f - n F_c) \quad (19)$$

Next, we will analyze how δ_{ε_k} affects the distribution characteristics of the EMI spectrum. The probability density of δ_{ε_k} with the former three chaotic signals, as shown in Fig. 11. By comparing Fig. 9 and Fig. 11, when the distribution range of δ_{ε_k} is smaller, it can be obtained that the magnitude of the spectrum is becoming lower, and the SBW is becoming smaller. Thus, the distribution of δ_{ε_k} could reflect the spectrum distribution of $v_{ds}(t)$ more accurately.

However, δ_{ε_k} still cannot be directly used as an impact factor of spectral distribution because δ_{ε_k} is a sequence that varies with the ε_k . Thus, it is necessary to define a parameter to weight the overall distribution regularity of δ_{ε_k} as the impact factor. In this paper, ARV is firstly defined, namely, the average relative variation of adjacent sequences in P cycle, as expressed in (20).

$$ARV = \frac{1}{P} \sum_{k=1}^P |\delta_{\varepsilon_k}| \quad (20)$$

The ARV are calculated for the former three cases, *Case I*: $ARV = 0.552$ when $T_{samp} = 1.0s$, *Case II*: $ARV = 0.164$ when $T_{samp} = 0.2s$, and *Case III*: $ARV = 0.019$ when $T_{samp} = 0.02s$. When the ARV decreases, it can be concluded that the magnitude of the $v_{ds}(t)$ spectrum is becoming lower, and the

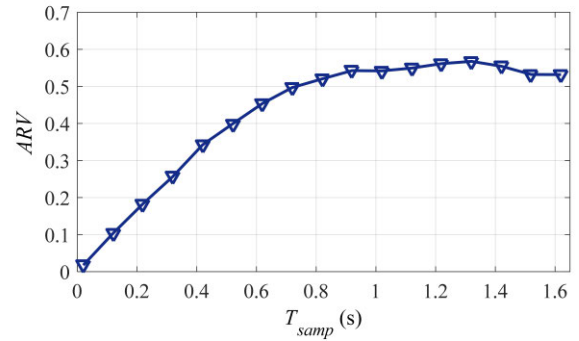


FIGURE 12. Changing curve of ARV with sampling period T_{samp} .

SBW is becoming smaller. More data will be analyzed below to verify this conclusion.

The more multi-scroll chaotic signals ε_k are also generated by sampling the 2×2 -scroll attractor with different T_{samp} . It should be noted that the ε_k must be ergodic at $[-1, 1]$. The changing curve of ARV with the T_{samp} is shown in Fig. 12. When T_{samp} increases, the ARV increases linearly firstly and then gradually becomes constant.

The spectral characteristics of $v_{ds}(t)$ around the switching frequency under MC-PWM will be analyzed with eleven different values of ARV . Spectrum magnitude and SBW_1 are two parameters to be focused. Detailed relationship curve of spectra magnitude with ARV is shown in Fig.13, the magnitude of spectra gradually increases when the ARV increases. Moreover, the changing curve of SBW_1 with ARV is shown in Fig.14, which indicates that the SBW_1 is becoming wider when the ARV is larger.

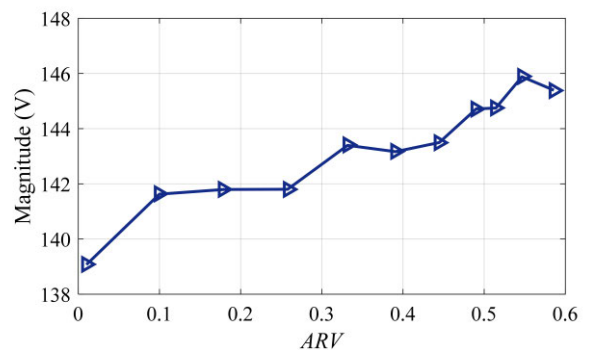


FIGURE 13. Changing curve of the maximum magnitude of $v_{ds}(t)$ spectra around the switching frequency with ARV .

To unify the spectral magnitude and SBW to one parameter expression, we define equivalent maximum energy (EME) to take into account both the magnitude and SBW of the spectrum, as shown in the (21), where A_{max_m} is the maximum magnitude of the spectrum around the $m \cdot f_{sw}$ under chaotic PWM.

$$EME_m \triangleq SBW_m \cdot A_{max_m}^2, \quad (m = 1, 2, 3 \dots). \quad (21)$$

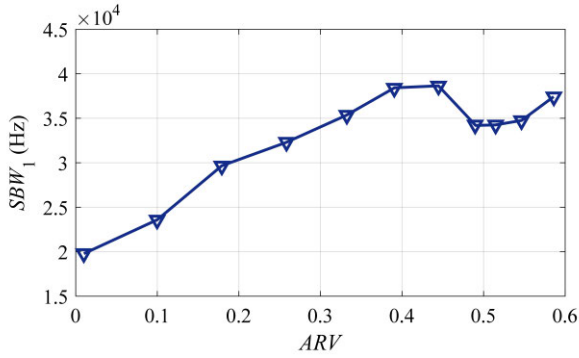


FIGURE 14. Changing curve of SBW_1 with ARV .

Further, in order to compare the EME_m directly under different switching frequency offset ΔF , load or output voltage, EME_m is normalized as EME_{pu_m} , as expressed in (22), where EME_{base_m} is the base value of the EME_m , $EME_{base_m} = m \cdot \Delta F \cdot A_{Tmax_m}^2$, A_{Tmax_m} is the maximum magnitude of the spectrum at the $m \cdot f_{sw}$ under T-PWM.

$$EME_{pu_m} = \frac{EME_m}{EME_{base_m}} = \frac{SBW_m \cdot A_{max_m}^2}{m \cdot \Delta F \cdot A_{Tmax_m}^2}, \quad (m = 1, 2, 3 \dots). \quad (22)$$

Therefore, EME_{pu_m} can be obtained by measuring the magnitude A_{max_m} and A_{Tmax_m} and calculating the SBW_m of the obtained spectra. The EME_{pu_m} at the switching frequency, namely, EME_{pu_1} , is selected in this paper to show the relationship between EME_{pu_m} and ARV . The EME_{pu_1} curve with the ARV is shown in Fig. 15 with a blue line. Further, the approximate expression of EME_{pu_1} versus ARV is obtained by using the fitting method, as expressed in (23). Moreover, the fitting curve of (23) is also plotted in Fig. 15 with a brown line. As the ARV increases, the EME_{pu_1} has a tendency to increase gradually, which indicates that it has better spectral characteristics when the ARV is smaller. More importantly, the selection method of chaotic signals for MC-PWM can be determined by the ARV .

$$EME_{pu_1} = 233.7 \cdot ARV^5 - 320.8 \cdot ARV^4 + 153.7 \cdot ARV^3 - 31.48 \cdot ARV^2 + 3.978 \cdot ARV + 0.2436, \quad ARV \in (0, 0.6). \quad (23)$$

According to the mechanism analysis of EMI spectral characteristics under MC-PWM, chaotic signals should be selected by comparing the ARV . The steps of selecting the chaotic signals method for MC-PWM are shown in Fig. 16, which will be described as follows.

- 1) Firstly, the topological structure of multi-scroll attractors needs to be determined according to (2).
- 2) Secondly, the range of T_{samp} should be determined.

The ε_k must be ergodic at $[-1, 1]$ by sampling the chaotic attractor with a minimum sampling period T_{samp_min} . Thus,

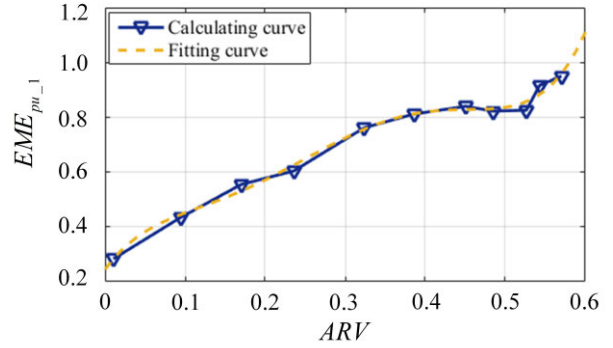


FIGURE 15. Changing curve of EME_{pu_1} with ARV .

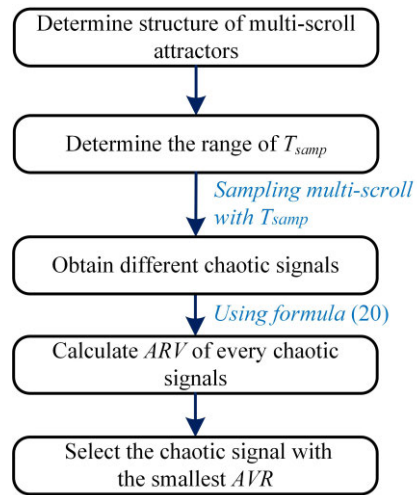


FIGURE 16. Flowchart of selecting chaotic signals method for MC-PWM.

the T_{samp_min} can be obtained with the approximate frequency f_{app} of the chaotic attractor and the P , as shown in (24), where the f_{app} could be identified by determining the frequency of the most significant magnitude in the spectrum of chaotic attractor.

$$T_{samp_min} = 1 / (P \cdot f_{app}) \quad (24)$$

Besides, the upper limit of the sampling period T_{samp_max} can be determined by selecting the T_{samp} corresponding to the inflexion point of the curve in Fig. 12. The ARV is almost constant when the T_{samp} is greater than the inflexion point, which means that the properties of the chaotic signals are almost identical.

- 3) Then, the different chaotic signals can be obtained from different T_{samp} with nT_{samp_min} ($n = 1, 2, 3 \dots [T_{samp_max}/T_{samp_min}]$).

4) The values of ARV of former chaotic signals can be further calculated using (20).

5) Finally, the chaotic signal with the smallest ARV will be selected to MC-PWM as a modulated signal to get a better spectral characteristic.

It should be noted that the selecting chaotic signals method can also be employed to TC-PWM with discrete chaotic mappings or other variable frequency PWM. The definitions of ARV and EME_{pu} in TC-PWM and other variable frequency PWM are the same as in MC-PWM. Therefore, this paper provides a method for comprehensively measuring the spread spectrum effect of all kinds of chaotic signals.

IV. SIMULATION ANALYSIS OF EMI SUPPRESSION UNDER MC-PWM

To verify the effectiveness of proposed MC-PWM on EMI suppression in power converters, and to verify the correctness of the given chaotic signal selection method in Section III, simulations have been carried out by MATLAB/Simulink based on the boost converter. The simulation parameters are given in TABLE 1. According to the analysis in Section III, the drain-source voltage v_{ds} of the switch Q is the EMI source, therefore, the spectra of v_{ds} is measured in simulations to compare the EMI distribution of the boost converter under different modulation methods.

The spectra of v_{ds} under T-PWM and TC-PWM are shown in Fig. 17, and the spectra of v_{ds} under MC-PWM with different ARV are shown in Fig. 18. It should be noted that logistic mapping is used in TC-PWM as a frequency modulation signal [33]. The logistic mapping can be expressed as (25).

$$\varepsilon_{k+1} = 1 - \lambda \varepsilon_k^2, \quad \varepsilon_k \in (-1, 1), \quad k = 1, 2, 3, \dots \quad (25)$$

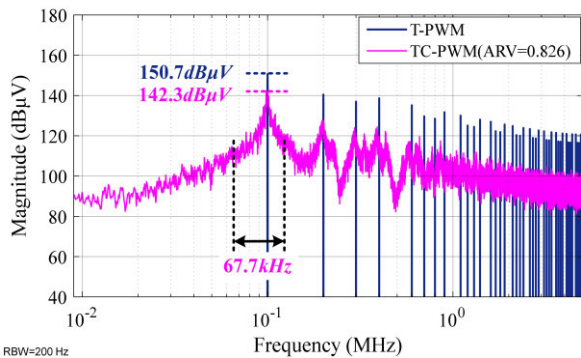


FIGURE 17. Simulation spectra of v_{ds} in a boost converter under different PWM.

From Fig. 17 and Fig. 18, TC-PWM and MC-PWM can reduce the magnitudes of EMI peaks distributed in switching frequency and its multiples a lot compared with T-PWM. However, the SBW_1 under TC-PWM is wider, which will result in sideband noises. MC-PWM could obtain more spectral characteristics by changing the chaotic signals to determine the optimal spectral distribution.

The quantitative comparison results of spectra of v_{ds} around the switching frequency are shown in TABLE 2. It can be concluded that when the ARV is smaller, the A_{max_1} is becoming smaller, the SBW_1 is becoming narrower, and the value of EME_{pu_1} is also becoming smaller correspondingly, which is consistent with the conclusion in the theoretical

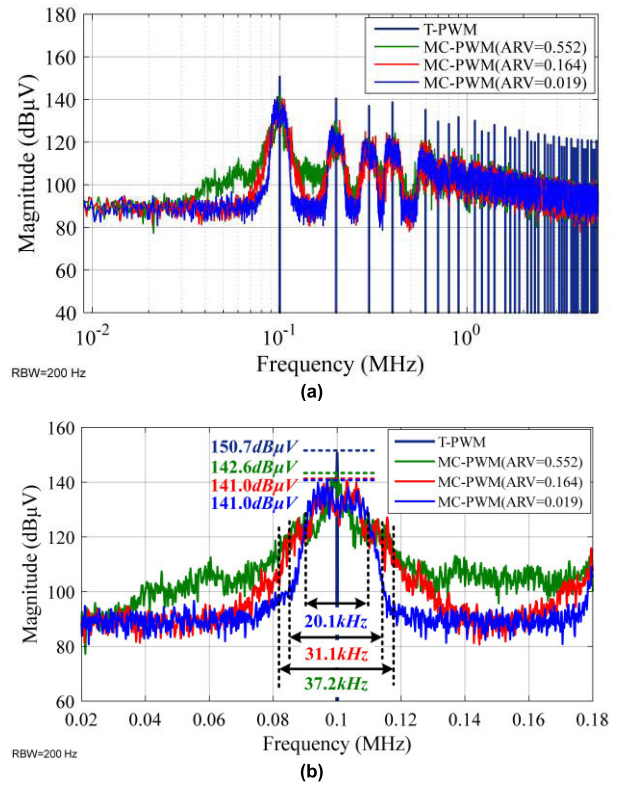


FIGURE 18. Simulation spectra of v_{ds} in a boost converter under MC-PWM with different ARV. (a) Frequency range 9kHz~5MHz. (b) Frequency range 20kHz~180kHz.

TABLE 2. Quantitative comparison results of simulation spectra.

Modulation Type	SBW_1 (kHz)	A_{max_1} (dBμV)	EME_{pu_1}
T-PWM	-	150.7	-
TC-PWM: ARV=0.826	67.7	142.3	1.79
MC-PWM Case I: ARV=0.552	37.2	142.6	1.01
MC-PWM Case II: ARV=0.164	31.1	141.0	0.73
MC-PWM Case III: ARV=0.019	20.1	141.0	0.47

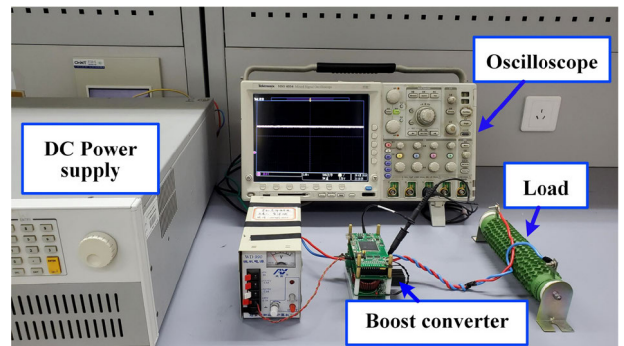


FIGURE 19. Experimental platform of the boost converter.

analysis of Section III. Therefore, it should choose the chaotic signal corresponding to $ARV = 0.019$ to achieve a better EMI suppression effect for power converters, which also verifies the correctness of the given chaotic signal selection method.

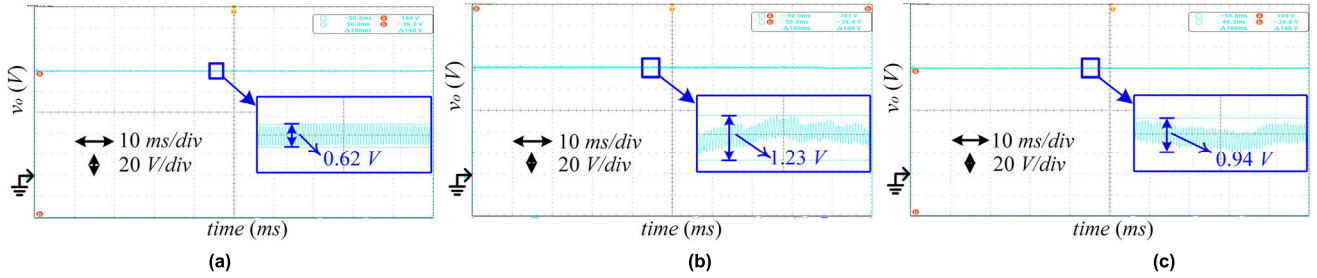


FIGURE 20. Output voltage waveform of the boost converter. (a) Under T-PWM. (b) Under TC-PWM. (c) Under MC-PWM with $ARV = 0.019$.

V. EXPERIMENTAL VERIFICATION

To further verify the effectiveness of EMI suppression using MC-PWM and the correctness of the chaotic signal selection method, a series of experiments were carried out based on the boost converter. The boost converter experimental platform is shown in Fig. 19, experimental parameters are listed in TABLE 3. All modulation methods are implemented by using Digital Signal Processor (DSP) TMS320F28035. The chaotic modulation signals ε_k in MC-PWM are generated by the difference expressions of discretizing the state variables of (2). Take the 2×2 -scroll attractor used in the paper as an example. Based on the Euler’s method, the difference expressions of (2) are shown in (26), where h_T should be set to the same as the sampling period T_{samp} .

$$\begin{cases} x(n+1) = x(n) + \alpha h_T \left\{ \begin{array}{l} y(n) + A_2 \cdot \text{sgn}(y(n)) \\ -\xi [x(n) + A_1 \cdot \text{sgn}(x(n))] \end{array} \right\} \\ y(n+1) = y(n) + h_T [x(n) - y(n) + z(n)] \\ z(n+1) = z(n) - \beta h_T [y(n) + A_2 \cdot \text{sgn}(y(n))] \end{cases} \quad (26)$$

TABLE 3. Main circuit parameters.

Parameter	Value
Input voltage	40 V
Output voltage	100 V
Inductor	100 μ H
Capacitor	300 μ F
Reference switching frequency	100 kHz
Rated power	300 W

Based on (26), it needs to define 12 variables in DSP programming. If the variables are defined as the long integer, they will take up 48 bytes of DSP space. The discrete state variables of 2×2 -scroll attractors can be obtained with DSP programming. Thus, the discrete state variables can be used as chaotic modulation signals ε_k , which will be applied to the generation of the chaotic carrier of the boost converter.

A. WORKING WAVEFORMS UNDER T-PWM AND CHAOTIC PWM

The output voltage waveforms of the boost converter under different modulation methods will be analysed first to ensure

that the MC-PWM does not affect the electrical characteristics of the boost converter, so as to ensure its normal work. Fig. 20 shows the output voltage waveforms of the boost converter under T-PWM, TC-PWM, and MC-PWM with $ARV = 0.019$. It can be seen that the output voltage ripple under TC-PWM and MC-PWM is higher compared with that under T-PWM. However, the ripples level are all below 1.5%, which can meet the output characteristics of the boost converter.

B. SPECTRAL CHARACTERISTICS UNDER T-PWM AND CHAOTIC PWM

Experimental spectra of v_{ds} under T-PWM and TC-PWM are shown in Fig. 21, and spectra of v_{ds} under MC-PWM with different ARV are shown in Fig. 22. The quantitative comparison results of v_{ds} spectra around the switching frequency are shown in TABLE 4. TC-PWM and MC-PWM both can reduce the magnitudes of EMI peaks a lot compared with T-PWM. However, the SBW_1 with MC-PWM is smaller compared with TC-PWM. For the MC-PWM with different ARV , the magnitude is becoming smaller, and the SBW_1 is becoming narrower when the ARV is smaller. This is consistent with the results of simulation and theoretical analysis.

In order to analyze the changing trend of the experimental EME_{pu-1} with ARV in detail, the change curve of EME_{pu-1} with ARV is shown in Fig. 23. When the ARV increases gradually, the EME_{pu-1} also increases, which is consistent with the theoretical analysis results of Fig. 15 in Section III. Thus, the given chaotic signal selection method for MC-PWM is correct.

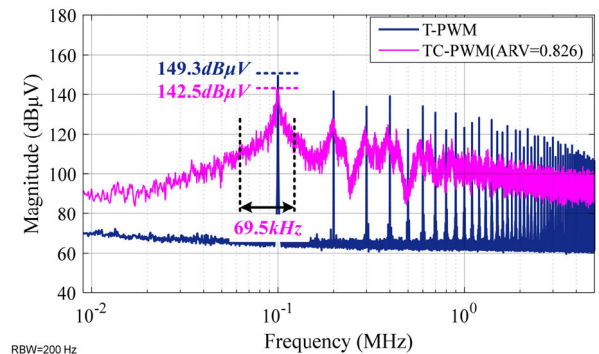


FIGURE 21. Experimental spectra of v_{ds} under different PWM.

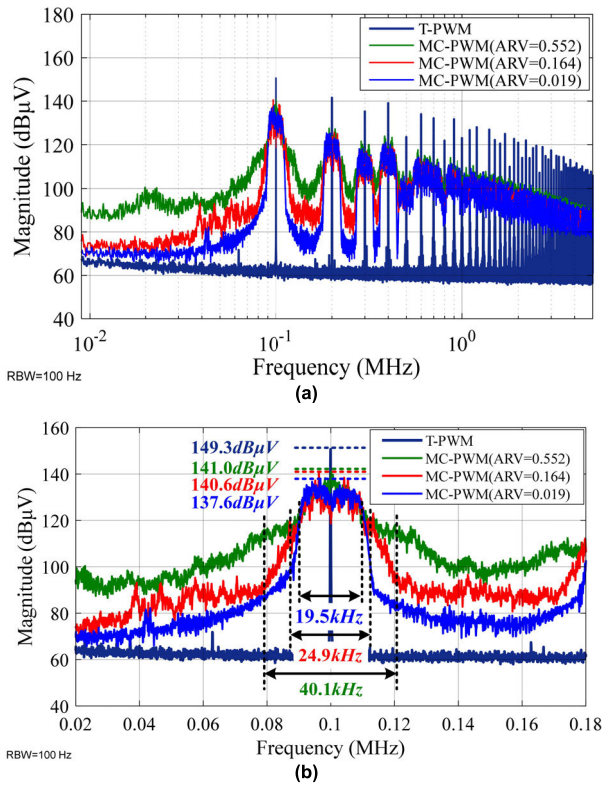


FIGURE 22. Experimental spectra of v_{ds} under MC-PWM with different ARV. (a) Frequency range 9kHz~5MHz. (b) Frequency range 20kHz~180kHz.

TABLE 4. Quantitative comparison results of experimental spectra.

Modulation Type	SBW_1 (kHz)	$A_{max,1}$ (dB μ V)	$EME_{pu,1}$
T-PWM	-	149.3	-
TC-PWM: $ARV=0.826$	69.5	142.5	2.05
MC-PWM Case I: $ARV=0.552$	40.1	141.0	1.03
MC-PWM Case II: $ARV=0.164$	24.9	140.6	0.62
MC-PWM Case III: $ARV=0.019$	19.5	137.6	0.35

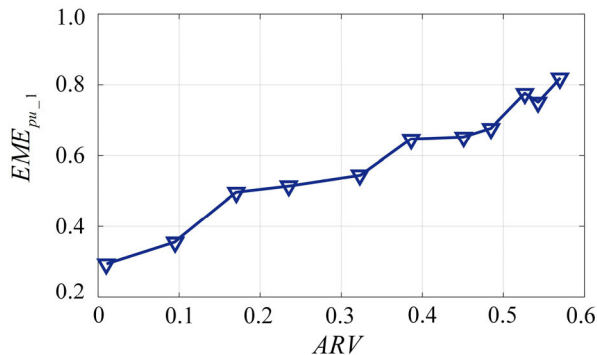


FIGURE 23. Experimental changing curve of $EME_{pu,1}$ with ARV.

C. RESULTS OF CONDUCTED EMI TEST

To further evaluate the EMI suppression effect of MC-PWM, the conducted EMI of the boost converter under T-PWM,

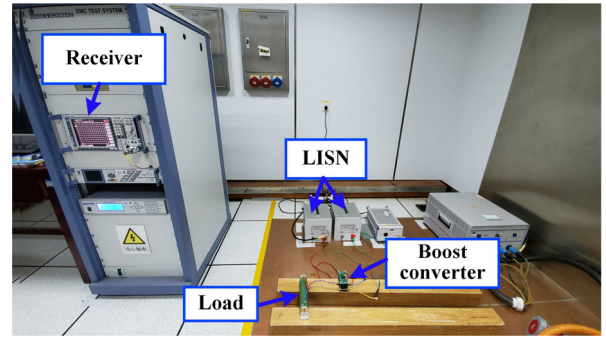


FIGURE 24. Experimental platform of conducted EMI of the boost converter.

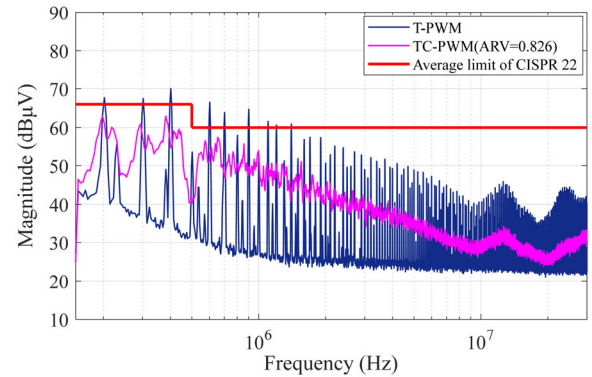


FIGURE 25. Conducted EMI test results under different PWM.

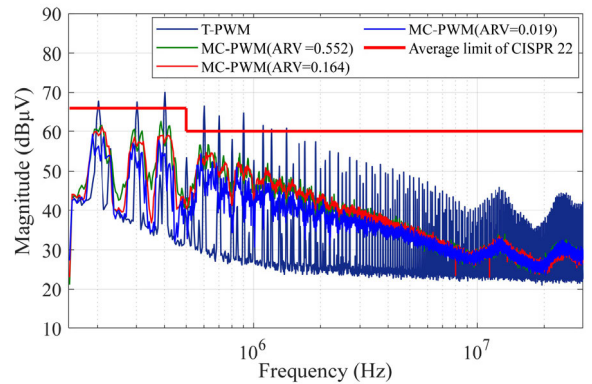


FIGURE 26. Conducted EMI test results under MC-PWM with different ARV.

TC-PWM and MC-PWM are measured. The measurement layout is shown in Fig. 24, the conducted EMI of the boost converter is measured through the line impedance stabilization network (LISN), and the receiver is R&S ESCI. The average values of conducted EMI results under T-PWM and TC-PWM from 150 kHz to 30MHz are shown in Fig. 25, the average values of conducted EMI results under MC-PWM with different ARV are presented in Fig. 26. To compare the magnitudes of conducted EMI in Fig. 25 and Fig. 26 more clearly, the maximum magnitudes of conducted EMI near the

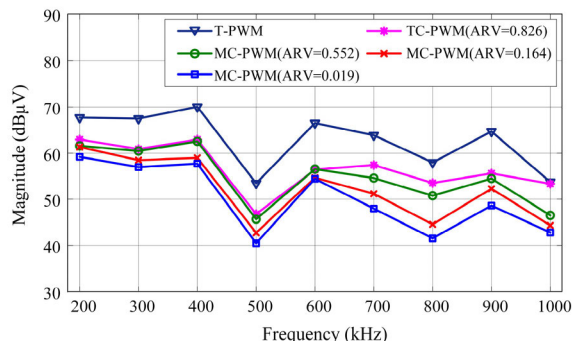


FIGURE 27. Comparison of maximum magnitudes of conducted EMI from 200kHz~1MHz.

switching frequency and its multiples under different PWM are shown in Fig. 27.

From Figs. 25-27, the magnitudes of EMI peaks under TC-PWM and MC-PWM are much lower than the magnitudes of EMI peaks under T-PWM. And the magnitudes of EMI peaks are smallest under MC-PWM with $ARV = 0.019$. Thus, the proposed MC-PWM has the advantages in suppressing EMI. More importantly, the chaotic signal determined by the chaotic signal selection method has the best EMI suppression effect, which also illustrates the correctness and effectiveness of the chaotic signal selection method.

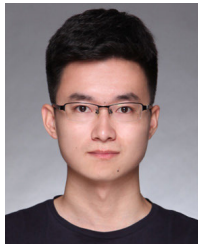
VI. CONCLUSION

In this paper, the continuous multi-scroll chaotic system is introduced into chaotic PWM to suppress EMI for power converters. Moreover, the influence mechanism of chaotic signals on the spectrum distribution of EMI is firstly analyzed, the selection method of chaotic signals is further obtained. It is noted that this method could be used to comprehensively measure the spread spectrum effect of all kinds of chaotic signals. Both simulation and experimental results prove the effectiveness of EMI suppression using MC-PWM and the correctness of the chaotic signal selection method. Therefore, the proposed MC-PWM provides a better EMI suppression way for power converters, and a chaotic signal selection method could provide the uniform evaluation criterion to guide the parameter design for chaotic PWM.

REFERENCES

- [1] K. Mainali and R. Oruganti, "Conducted EMI mitigation techniques for switch-mode power converters: A survey," *IEEE Trans. Power Electron.*, vol. 25, no. 9, pp. 2344–2356, Sep. 2010.
- [2] D. Han, C. T. Morris, W. Lee, and B. Sarlioglu, "A case study on common mode electromagnetic interference characteristics of GaN HEMT and Si MOSFET power converters for EV/HEVs," *IEEE Trans. Transport. Electrific.*, vol. 3, no. 1, pp. 168–179, Mar. 2017.
- [3] L. Xing and J. Sun, "Optimal damping of multistage EMI filters," *IEEE Trans. Power Electron.*, vol. 27, no. 3, pp. 1220–1227, Mar. 2012.
- [4] R. Goswami, S. Wang, E. Solodovnik, and K. J. Karimi, "Differential mode active EMI filter design for a boost power factor correction AC/DC converter," *IEEE J. Emerg. Sel. Topics Power Electron.*, vol. 7, no. 1, pp. 576–590, Mar. 2019.
- [5] R. Gamoudi, D. E. Chariag, and L. Sbita, "A review of spread-spectrum-based PWM Techniques—A novel fast digital implementation," *IEEE Trans. Power Electron.*, vol. 33, no. 12, pp. 10292–10307, Dec. 2018.
- [6] H. G. Li, S. D. Gong, J. W. Liu, and D. L. Su, "CMOS-based chaotic PWM generator for EMI reduction," *IEEE Trans. Electromagn. Compat.*, vol. 59, no. 4, pp. 1224–1231, Aug. 2017.
- [7] L. Premalatha and T. A. Raghavendiran, "A simple approach of generating CPWM for reducing conducted emission in switched mode power supplies," *IEEE Electromagn. Compat. Mag.*, vol. 2, no. 4, pp. 67–71, 4th Quart., 2013.
- [8] K. K. Tse, R. W.-M. Ng, H. S.-H. Chung, and S. Y. R. Hui, "An evaluation of the spectral characteristics of switching converters with chaotic carrier-frequency modulation," *IEEE Trans. Ind. Electron.*, vol. 50, no. 1, pp. 171–182, Feb. 2003.
- [9] Z. Wang, B. Liu, L. Guan, Y. Zhang, M. Cheng, B. Zhang, and L. Xu, "A dual-channel magnetically integrated EV chargers based on double-stator-winding permanent-magnet synchronous machines," *IEEE Trans. Ind. Appl.*, vol. 55, no. 2, pp. 1941–1953, Mar. 2019.
- [10] Y. Song and J. Niu, "Application of chaotic pulse width modulation control for suppressing electromagnetic interference in a half-bridge converter," *J. Eng.*, vol. 2014, no. 8, pp. 487–493, Aug. 2014.
- [11] R. Mukherjee, A. Patra, and S. Banerjee, "Impact of a frequency modulated pulsewidth modulation (PWM) switching converter on the input power system quality," *IEEE Trans. Power Electron.*, vol. 25, no. 6, pp. 1450–1459, Jun. 2010.
- [12] F. Pareschi, G. Setti, R. Rovatti, and G. Frattini, "Short-term optimized spread spectrum clock generator for EMI reduction in switching DC/DC converters," *IEEE Trans. Circuits Syst. I, Reg. Papers*, vol. 61, no. 10, pp. 3044–3053, Oct. 2014.
- [13] H. Li, Z. Li, F. Lin, and B. Zhang, "Suppressing harmonics in four-quadrant AC-DC converters with chaotic SPWM control," *Int. J. Circuit Theory Appl.*, vol. 42, no. 4, pp. 331–342, Apr. 2014.
- [14] Z. Wang, K. T. Chau, and C. Liu, "Improvement of electromagnetic compatibility of motor drives using chaotic PWM," *IEEE Trans. Magn.*, vol. 43, no. 6, pp. 2612–2614, Jun. 2007.
- [15] H. Li, Y. Ding, Z. Yang, and Y. Jiang, "Optimization design of EMI filter with chaotic PWM in DC-DC converters," in *Proc. IEEE Workshop Wide Bandgap Power Devices Appl. Asia (WiPDA Asia)*, Taipei, Taiwan, May 2019, pp. 1–6.
- [16] H. Li, Y. Liu, J. Lu, T. Zheng, and X. Yu, "Suppressing EMI in power converters via chaotic SPWM control based on spectrum analysis approach," *IEEE Trans. Ind. Electron.*, vol. 61, no. 11, pp. 6128–6137, Nov. 2014.
- [17] R. Yang, B. Zhang, D. Qiu, and Z. Liu, "Time-frequency and wavelet transforms of EMI dynamic spectrum in chaotic converter," *IEEE Trans. Power Electron.*, vol. 24, no. 4, pp. 1083–1092, Apr. 2009.
- [18] F. Pareschi, R. Rovatti, and G. Setti, "EMI reduction via spread spectrum in DC/DC converters: State of the art, optimization, and tradeoffs," *IEEE Access*, vol. 3, pp. 2857–2874, Dec. 2015.
- [19] H. Li, Z. Yang, B. Wang, V. G. Agelidis, and B. Zhang, "On thermal impact of chaotic frequency modulation SPWM techniques," *IEEE Trans. Ind. Electron.*, vol. 64, no. 3, pp. 2032–2043, Mar. 2017.
- [20] Z. Yang, H. Li, F. Lin, B. Zhang, and J. Lu, "Common-mode electromagnetic interference calculation method for a PV inverter with chaotic SPWM," *IEEE Trans. Magn.*, vol. 51, no. 11, pp. 1–4, Nov. 2015.
- [21] H. Li, Z. Yang, D. Yang, X. Gao, and J. Lu, "Suppressing electromagnetic interference of power converters based on 2×2 -scroll chaotic PWM method," in *Proc. IEEE Magn. Conf. (INTERMAG)*, Beijing, China, May 2015, p. 1.
- [22] G. Chen and J. Lü, *Dynamics Analysis, Synchronization and Control of Lorenz Family*. Beijing, China: Science Press, 2003.
- [23] L. Chua, M. Komuro, and T. Matsumoto, "The double scroll family," *IEEE Trans. Circuits Syst.*, vol. 33, no. 11, pp. 1072–1118, Nov. 1986.
- [24] G. Chen and T. Ueta, "Yet another chaotic attractor," *Int. J. Bifurcation Chaos*, vol. 9, no. 7, pp. 1465–1466, Jul. 1999.
- [25] J. Lü and G. Chen, "A new chaotic attractor coined," *Int. J. Bifurcation Chaos*, vol. 12, no. 03, pp. 659–661, Mar. 2002.
- [26] A. M. Rucklidge, "Chaos in models of double convection," *J. Fluid Mech.*, vol. 237, pp. 209–229, Apr. 1992.
- [27] S. Yu, *Chaotic Systems and Chaotic Circuits: Principle Design and Its Application in Communications*. Xian, China: Xidian Univ. Press, 2011.
- [28] S. Yu, K. S. Tang, and G. Chen, "Generation of $n \times m$ -scroll attractors under a Chua-circuit framework," *Int. J. Bif. Chaos*, vol. 17, no. 11, pp. 3951–3964, 2007.

- [29] H. Li, Z. Li, B. Zhang, F. Wang, N. Tan, and W. A. Halang, "Design of analogue chaotic PWM for EMI suppression," *IEEE Trans. Electromagn. Compat.*, vol. 52, no. 4, pp. 1001–1007, Nov. 2010.
- [30] Y. Liu, H. Li, B. Zhang, T. Zheng, and X. You, "Spectrum calculation of chaotic SPWM signals based on double Fourier series," *Acta Phys. Sin.*, vol. 63, no. 7, pp. 1–10, Apr. 2014.
- [31] H. Chen, T. Wang, L. Feng, and G. Chen, "Determining far-field EMI from near-field coupling of a power converter," *IEEE Trans. Power Electron.*, vol. 29, no. 10, pp. 5257–5264, Oct. 2014.
- [32] C. Phillips, J. Parr, and E. Riskin, *Signals, Systems, and Transforms*. New York, NY, USA: Pearson, 2013.
- [33] R. Gamoudi, D. Chariag, and L. Sbita, "Electromagnetic interference reduction in boost converter using logistic PWM," in *Proc. Int. Conf. Green Energy Convers. Syst. (GECS)*, Hammamet, Tunisia, Mar. 2017, pp. 1–4.



ZHICHANG YANG (Graduate Student Member, IEEE) was born in Chifeng, China, in 1991. He received the B.S. degree in electrical engineering from Beijing Jiaotong University, Beijing, China, in 2013, where he is currently pursuing the Ph.D. degree in electrical engineering with the School of Electrical Engineering.

He has published more than ten articles and applied 12 patents. His current research interests include power electronics, electromagnetic interference, stability analysis, and chaos control and its applications.



HONG LI (Senior Member, IEEE) received the B.Sc. degree from the Taiyuan University of Technology, Taiyuan, China, in 2002, the M.Sc. degree from the South China University of Technology, Guangzhou, China, in 2005, and the Ph.D. degree from the FernUniversität in Hagen, Hagen, Germany, in 2009.

She is currently a Professor with the School of Electrical Engineering, Beijing Jiaotong University, Beijing, China. She has published one book, 36 journal articles, and 45 conference papers. She has also applied 24 patents. Her research interests include nonlinear modeling, analysis, and its applications, EMI suppressing methods for power electronic systems, and wide bandgap power devices and applications.

Dr. Li is the Vice Chairman of the Electromagnetic Compatibility Specialized Committee in China Power Supply Society. She is an Associate Editor of the IEEE TRANSACTIONS ON INDUSTRIAL ELECTRONICS and the *Chinese Journal of Electrical Engineering*.



YUHANG DING was born in Anhui, China, in 1995. He received the B.S. degree in electrical engineering from Beijing Jiaotong University, Beijing, China, in 2018, where he is currently pursuing the M.S. degree in electrical engineering with the School of Electrical Engineering.

His current research interest includes electromagnetic compatibility in power electronics.



JIAXIN WANG was born in Shanxi, China, in 1996. He received the B.S. degree in electrical engineering from the Taiyuan University of Technology, Shanxi, in 2018. He is currently pursuing the M.S. degree in electrical engineering with the School of Electrical Engineering, Beijing Jiaotong University, Beijing, China.

His current research interest includes electromagnetic compatibility in power electronics.

...